Bub1 availability limits the Spindle Assembly Checkpoint signaling strength of human kinetochores

Chu Chen[1,2], Lauren Humphrey[1], Soubhagyalaxmi Jema[1], Frank Ferrari[1], Ajit P. Joglekar[1,2]

1 - Department of Cell and Developmental Biology, University of Michigan Medical School, Ann Arbor, Michigan 48109

2 - Department of Biophysics, University of Michigan, Ann Arbor, Michigan 48109

Corresponding author: ajitj@umich.edu

Abstract

The Spindle Assembly Checkpoint (SAC) is activated by unattached or laterally attached kinetochores in a dividing cell. It delays anaphase onset and thus prevents chromosome missegregation. To minimize chromosome missegregation, the last signaling kinetochore in the cell must produce the anaphase-inhibitory signal at a high rate to delay anaphase onset. Additionally, the large number of signaling kinetochores should be prevented from generating an unnecessarily large signal. How the cell balances these conflicting requirements remains unclear. Here, we show that the number of SAC proteins recruited by an unattached kinetochore is inversely correlated with the number of unattached kinetochores in HeLa cells. This correlation primarily results from the low amount of the protein Bub1, and this protein recruitment shortfall reduces the signaling activity of the kinetochore enabling chromosome missegregation. Conversely, Bub1 overexpression results in higher SAC protein recruitment and longer delays. Thus, the regulation of the signaling activity of unattached kinetochores by mass action kinetics promotes accurate chromosome segregation.

Running title: Changing signaling strength of the kinetochore

Introduction

To ensure accurate chromosome segregation during mitosis, a dividing cell must not enter anaphase until all of its chromosomes are stably attached to the mitotic spindle. Such conditional entry into anaphase is enforced by a cell cycle control known as the Spindle Assembly Checkpoint (SAC). The SAC is activated by unattached or laterally attached kinetochores, which recruit several signaling proteins and produce the 'Mitotic Checkpoint Complex' (MCC) (Lara-Gonzalez et al., 2021b; Musacchio, 2015). The MCC inhibits the Anaphase-Promoting Complex/Cyclosome (APC/C) and thus delays anaphase onset (Izawa and Pines, 2015; Sudakin et al., 2001). This delay ensures accurate chromosome segregation by enabling the unattached kinetochores to attach to spindle microtubules.

The relationship between the amount of the MCC and the decreasing number of signaling kinetochores in a dividing cell is likely to influence the effectiveness of the SAC in minimizing chromosome missegregation. This relationship will be especially important in human cells, wherein the number of unattached kinetochores drops by almost two orders of magnitude: from ~ 92 following nuclear envelop break-down (NEBD) to a few or just one in prometaphase. Anaphase must not commence irrespective of the number of unattached kinetochores in the cell, and to meet this condition, the amount of the MCC in the cell must remain above the threshold amount required to prevent anaphase onset. If there is a direct scaling between the number of unattached kinetochores and the amount of MCC in the cell, the nearly 100-fold drop in the number of kinetochores will result in a similar drop in the MCC amount (Clute and Pines, 1999; Dick and Gerlich, 2013). This drop will be problematic if the signaling output of a single kinetochore is insufficient to delay anaphase onset.

A direct scaling between the number of unattached kinetochores and the amount of MCC in the cell can be averted by a simple mechanism. Unattached kinetochores assemble the MCC by recruiting SAC signaling proteins via a well-defined signaling cascade (Figure 1A) (Faesen et al., 2017; Ji et al., 2017; Lara-Gonzalez et al., 2021a; London and Biggins, 2014; London et al., 2012; Piano et al., 2021; Primorac et al., 2013; Shepperd et al., 2012). Furthermore, SAC strength is correlated with the amount of SAC signaling proteins that the kinetochores recruit (Collin et al., 2013; Vleugel et al., 2015). Given these two observations, mass action kinetics of SAC protein binding to the kinetochore can avert direct scaling between the number of signaling kinetochores and the cumulative amount of MCC in the cell. As the number of unattached kinetochores drops, the availability of SAC signaling proteins will proportionately increase, enabling the remaining unattached kinetochores to recruit more signaling proteins and generate MCC at a higher rate. In

other words, the signaling strength of each kinetochore will become inversely correlated to the number of signaling kinetochores in the cell. Such a correlation can be an important mechanism in approximating switch-like activation of the SAC with respect to the number of signaling kinetochores (Chen et al., 2019). However, whether this correlation exists in human cells, and if so, the factors that establish it remains unknown.

Here, we characterize the dependence of the signaling strength of signaling kinetochores on the number of signaling kinetochores in HeLa cells. For this, we use fluorescence microscopy to quantify the amount of three SAC signaling proteins in genome-edited HeLa cell lines that express fluorescently tagged versions of the three proteins. Our data provide new insights into the regulation of SAC signaling strength of HeLa kinetochores.

Results

Dependence of the copy number of SAC proteins recruited per signaling kinetochore on the number of signaling kinetochores in the cell

The SAC signaling cascade is activated when the kinetochore protein Knl1 is phosphorylated by the Mps1 kinase at the 'MELT' motifs, so called because of their consensus amino acid sequence (Primorac et al., 2013; Tromer et al., 2015; Vleugel et al., 2013). Each MELT motif serves as the scaffold for recruiting downstream signaling proteins (Chen et al., 2019; Primorac et al., 2013). Prior studies in human cells have shown that the strength of the SAC is weakly correlated with the number of MELT motifs in Knl1 and the amount of SAC proteins that they recruit (Vleugel et al., 2015; Vleugel et al., 2013; Zhang et al., 2014). The cumulative MCC generated is also correlated with the number of signaling kinetochores (Collin et al., 2013; Dick and Gerlich, 2013). To better characterize these correlations, we decided to quantify the copy number of SAC proteins recruited by individual signaling kinetochores to assess their steady state signaling activity. We selected one protein each from the three-layered recruitment cascade: Bub1, BubR1, and Mad1. Bub1 recruits BubR1, the Mad1-Mad2 complex, and Cdc20 (Lara-Gonzalez et al., 2021a; Piano et al., 2021), BubR1 an essential MCC component, and Mad1 helps catalyze the conformational change in Mad2 during MCC formation (Mapelli et al., 2007).

To ensure accurate quantification and comparative analysis, we used genome-edited HeLa cells that express either mNeonGreen-Bub1, mNeonGreen-BubR1, or Mad1-mNeonGreen ["mNeonGreen" is abbreviated as "mNG" henceforth; (Shaner et al., 2013)]. Because the fluorescent tags are separated from the tagged proteins by flexible linkers, and we have

90 previously found that N-terminally tagged BubR1 and C-terminally tagged Mad1 are functional in
91 budding yeast (Aravamudhan et al., 2016; Roy et al., 2022). Because of the similarity of the
92 domain organizations of Bub1 and BubR1, we expect that Bub1 function will also be unaffected
93 by the N-terminal tag. In our genome-edited HeLa cells, about half of the total protein is
94 fluorescently labeled; the remaining protein is unlabeled (Banerjee et al., 2021). Therefore, we
95 assume that signaling kinetochores recruit approximately equal amounts of the labeled and
96 unlabeled proteins. In the measurements presented, we double the number of mNG-labeled
97 proteins to estimate the total number of molecules recruited by the signaling kinetochores.

98 Our first goal was to characterize the dependence of Bub1, BubR1, and Mad1 recruitment per
99 kinetochore on the number of signaling kinetochores in the cell. To attain this goal, we observed
100 mitotically arrested cells containing two distinctly different numbers of signaling kinetochores. To
101 obtain cells with nearly all kinetochores unattached, we released G1/S arrested HeLa cells into
102 the cell cycle and then arrested them in mitosis using 330 nM nocodazole, a drug that
103 depolymerizes microtubules (Figure 1B, right). These cells serve as a model for cells right after
104 NEBD. To obtain mitotic cells with a much smaller number of signaling kinetochores, we released
105 G1/S arrested HeLa cells into the cell cycle and treated them with 236 nM GSK923295, a small
106 molecule inhibitor of the mitotic kinesin CENP-E, 1.5 hours prior to imaging (Qian et al., 2010). In
107 these cells, which model prometaphase, most chromosomes align at the metaphase plate, and
108 their kinetochores recruit very low amounts of SAC proteins (Figure 1B, left). A smaller, variable
109 number of chromosomes become stranded at the spindle poles with either unattached or laterally
110 attached kinetochores that activate the SAC (Figure 1B, left) (Krefman et al., 2015; Kuhn and
111 Dumont, 2019). We analyzed only those cells containing ~ 10 or less polar chromosomes based
112 on a visual inspection of the image stacks.

113 To estimate the number of molecules from the measured mNG signal per kinetochore, we also
114 imaged HeLa cells exogenously expressing Spc25-mNG under identical imaging conditions and
115 quantified the Spc25-mNG signal per kinetochore (Figure 1C, right). Spc25 is a subunit of the
116 Ndc80 complex, and it is known that: (a) the human kinetochore contains ~ 250 molecules of the
117 Ndc80 complex and (b) the stoichiometry between Ndc80 and Knl1 is 3:2 (Suzuki et al., 2015).
118 This information allowed us to estimate the number of each SAC protein per Knl1 and relate it to
119 the number of MELT motifs per Knl1.

120 We first examined the SAC protein recruitment in cells treated with nocodazole (gray circles in
121 Figure 1C, left). Using the calibration standard above, we estimate that in cells containing many
122 signaling kinetochores each Knl1 molecule recruits only 2.3 ± 1.1 Bub1 molecules (mean ± std.

123 dev., Figure 1D). This number is lower than the previously reported value between four and six,
124 possibly because the expression level of exogenous, labeled Bub1 may have been higher than
125 physiological levels (Vleugel et al., 2015). BubR1 and Mad1 recruitment per kinetochore in
126 nocodazole-treated cells was lower than the Bub1 recruitment (1.5 ± 0.9 and 1 ± 0.9 molecule per
127 Knl1 of BubR1 and Mad1 respectively). Given that Knl1 contains 19 putative MELT motifs with
128 different Bub1- Bub3 binding affinities, these results show that each kinetochore uses only a
129 fraction of its maximal signaling capacity as shown previously (Vleugel et al., 2015; Vleugel et al.,
130 2013; Zhang et al., 2014). This is also the case in budding yeast (Aravamudhan et al., 2016).

131 We next quantified the recruitment of the three SAC proteins in GSK923295-treated cells
132 containing far fewer signaling kinetochores (orange circles in Figure 1C, left). In these cells,
133 protein recruitment per kinetochore was significantly higher: the number of Bub1 molecules per
134 kinetochore increased to 3.3 ± 1.5; the number of BubR1 and Mad1 molecules per kinetochore
135 was equal to Bub1 (3.5 ± 1.3 and 2.7 ± 1.2 per kinetochore, respectively). Taken together with
136 the data from nocodazole-treated cells, these measurements suggest that the number of SAC
137 proteins recruited per kinetochore is inversely correlated with the number of signaling
138 kinetochores in the cell. Furthermore, all three proteins are recruited in approximately equal
139 amounts. This trend is also consistent with observations of Bub1 and Mad1 recruitment in budding
140 yeast kinetochores (Aravamudhan et al., 2016).

141 Mad1-Mad2 is recruited to metazoan kinetochores by Bub1 and the RZZ complex (Pereira et al.,
142 2018; Rodriguez-Rodriguez et al., 2018; Silio et al., 2015). To quantify the contribution of the RZZ
143 complex, we depleted *ZW10* using RNA interference (RNAi) and then quantified SAC protein
144 recruitment as before. *ZW10* siRNA treatment resulted in a ~ 25% decrease in Bub1 and BubR1
145 recruitment, as noted by others (Kops et al., 2005). As expected, Mad1 recruitment was
146 significantly lower in both GSK923295 and nocodazole-treated cells (Figure S1). The number of
147 Mad1 molecules recruited per Bub1 molecule was reduced by ~ 50% revealing the contribution
148 of the RZZ under these conditions. Although the number of Bub1 and BubR1 molecules per
149 kinetochore was also reduced, the two proteins were recruited in approximately equal amounts.

150

151 **Mps1-mediated phosphorylation within signaling kinetochores is the same in nocodazole-**
152 **and GSK923295-treated cells**

153 The observed difference in the recruitment of SAC proteins per kinetochore in the nocodazole-
154 and GSK923295-treated cells may be due to a change in the phosphoregulation of the

155 kinetochore. To test this hypothesis, we quantified the net Mps1-mediated phosphorylation within
156 the kinetochore using a recently developed FRET-based sensor of Mps1 kinase activity that is
157 fused to the N-terminus of the kinetochore subunit Spc24 (Kuijt et al., 2020). We modified this
158 sensor to use mNeonGreen/mScarlet-I as the acceptor/donor combination (Figure 2A-B, Figure
159 S2). Since the acceptor and the donor has a fixed 1:1 stoichiometry in the sensor, we used the
160 ratio of the green channel readout and the raw FRET channel readout (without correcting for the
161 cross-excitation of the acceptor fluorescence and the bleed-through of donor fluorescence) as the
162 normalized measurement of the FRET efficiency and hence the net Mps1-mediated
163 phosphorylation.

164 We confirmed that MPS1sen-KT recruited to unaligned kinetochores in both nocodazole- and
165 GSK923295- treated cells had lower FRET efficiencies (higher activities of Mps1) compared to
166 kinetochores aligned at metaphase plates in GSK923295-treated cells (Figure S2). Importantly,
167 we did not detect any difference in the net Mps1-mediated phosphorylation within unaligned
168 kinetochores in nocodazole- and GSK923295-treated cells irrespective of the drug concentration
169 used (Figure 2C). Therefore, the difference in the recruitment of SAC proteins per kinetochore in
170 nocodazole- and GSK923295-treated cells is likely to be due to a competition for the limited pool
171 of SAC protein. This observation contrasts with the previous report that the average localization
172 levels of endogenously tagged HA-mCherry-Bub1 to signaling kinetochores in a CRISPR-Cas9-
173 edited HeLa cell line treated with either 250 nM of GSK923295 or 6.6 μM of nocodazole were not
174 significantly different (Kuijt et al., 2020). One possible explanation is that the much higher
175 concentration of nocodazole in the aforementioned study contributes to a more complete
176 breakdown of spindles and a higher degree of phosphorylation of MELT motifs, whereas in the
177 GSK923295-treated cells, the lack of filtering of based on the number of unaligned chromosomes
178 would lead to similar average numbers of signaling kinetochores in the Nocodazole- and
179 GSK923295-treated cells. We also cannot rule out the possibility that the differences reflect
180 different Bub1 expression levels or kinase/phosphatase activities in the HeLa cell lines used.

181

182 **The number of MELT motifs per Knl1 influences the recruitment of Bub1, BubR1, and Mad1**
183 **to signaling kinetochores**

184 Given that differences in the phosphoregulation of signaling kinetochores cannot explain the
185 observed differences in SAC protein recruitment, we studied the influence of the number of MELT
186 motifs in Knl1 on the recruitment of SAC proteins. For this study, we knocked down endogenous
187 Knl1 using RNAi and replaced it with recombinant, mScarlet-I-tagged versions of Knl1 containing

188 three or six MELT motifs: Knl1$^{\Delta}$-M3 or Knl1$^{\Delta}$-M3-M3 (Figure 3A, top) (Vleugel et al., 2015). As
189 before, we quantified Bub1, BubR1, and Mad1 signals at individual kinetochores in cells treated
190 with either GSK923295 or nocodazole (Figure 3B). For comparing the amounts of proteins
191 recruited under these conditions, we used the average mNG-Bub1 fluorescence signal per
192 kinetochore in nocodazole-treated cells expressing Knl1$^{\Delta}$-M3 as the basis, because it was
193 expected to be the lowest signal (Figure 1).

194 Quantification of protein recruitment revealed interesting trends. In nocodazole-treated cells,
195 Knl1$^{\Delta}$-M3-M3 recruited ~ 1.3-fold more mNG-Bub1 per kinetochore compared to Knl1$^{\Delta}$-M3 (Figure
196 3B, left, also see Figure S3A). In GSK923295-treted cells, Knl1$^{\Delta}$-M3 and Knl1$^{\Delta}$-M3-M3 recruited
197 ~ 1.4-fold and 2-fold more mNG-Bub1 per kinetochore than Knl1$^{\Delta}$-M3 in the nocodazole-treated
198 cells. These observations indicate that: (1) each Knl1$^{\Delta}$-M3 likely recruits < 3 Bub1 molecules in
199 nocodazole-treated cells, which is consistent with our estimation of the number of Bub1 molecules
200 per Knl1, (2) Knl1$^{\Delta}$-M3-M3 recruits more Bub1 than Knl1$^{\Delta}$-M3 under both conditions (Vleugel et
201 al., 2015), and (3) mNG-Bub1 recruitment per kinetochore is significantly higher for both versions
202 of Knl1 in the GSK923295-treated cells. The recruitment of Mad1-mNG per kinetochore exhibited
203 a similar trend as mNG-Bub1 (Figure 3B, right). The difference in mNG-BubR1 recruitment per
204 kinetochore by the two Knl1 versions was striking: Knl1$^{\Delta}$-M3-M3 recruited twice as much mNG-
205 BubR1 per kinetochore as Knl1$^{\Delta}$-M3 in the nocodazole- and GSK923295-treated cells (Figure 3B,
206 middle panel).

207 These observations provide the following insights into the recruitment of SAC proteins to the
208 kinetochore. First, the number of MELT motifs per Knl1 strongly influences the number of SAC
209 proteins recruited per kinetochore to a limit. Second, this influence is clearly visible in cells
210 containing small numbers of unattached kinetochores. The likely factor responsible for the lower-
211 than-expected recruitment of SAC proteins is their depletion from the cytoplasm. Given that Bub1-
212 Bub3 is the first protein complex recruited by the MELT motifs (Figure 1A), the expression level
213 of Bub1 emerges as a critical, limiting factor. Mad1 expression level in the HeLa cells is similar to
214 that of Bub1 suggesting that it may also limit its own recruitment (Banerjee et al., 2021).
215 Interestingly, Knl1$^{\Delta}$-M3-M3 recruits roughly twice as much BubR1 as Knl1$^{\Delta}$-M3 under both
216 conditions. The reasons behind this remain unclear; it is possible that BubR1 binds
217 phosphorylated MELT motifs directly (Zhang et al., 2016).

218 To test whether the cytoplasmic pool of mNG-Bub1 is depleted in nocodazole-treated cells, we
219 used Fluorescence Correlation Spectroscopy (FCS). Using FCS, we quantified the cytoplasmic
220 abundance of the two proteins in cells arrested in metaphase due to MG132 treatment and cells

221 treated with nocodazole (Methods). These measurements showed that cytosolic concentration of
222 Bub1 is significantly lower in nocodazole-treated compared to MG132-treated cells (Figure S3B).
223 In contrast, the concentration of cytoplasmic mNG-BubR1 was not significantly different under the
224 two conditions. Due to the potential complications associated with the heterodimerization of
225 Mad1-mNG with untagged, endogenous Mad1 prevented, we did not analyze FCS data for Mad1-
226 mNG (now shown).

227

228 **Higher recruitment of SAC proteins to the kinetochore correlates with longer delays in**
229 **anaphase onset**

230 Whether the higher recruitment of SAC proteins by Knl1$^{\Delta}$-M3-M3 translates into a stronger SAC
231 and longer mitotic arrest durations is a key question. Previous studies concluded that the number
232 of MELT motifs per Knl1 does not influence the duration of SAC-mediated mitotic arrest (Vleugel
233 et al., 2015; Zhang et al., 2014). The likely explanation for this finding is that these studies
234 characterized SAC signaling only in cells treated with high doses of nocodazole. Our
235 quantification shows that in the nocodazole-treated cells, kinetochores containing Knl1$^{\Delta}$-M3-M3
236 recruit on average only 20% higher amounts of Bub1 and Mad1 compared to kinetochores
237 containing Knl1$^{\Delta}$-M3. Therefore, the average duration of the nocodazole-induced mitotic arrest
238 may have been similar following nocodazole treatment. A further complicating factor is that one
239 of the studies partially inhibited Mps1 as an experimental convenience, which may have masked
240 differences in SAC signaling due to the two Knl1 versions (Vleugel et al., 2015).

241 Based on these considerations, we measured the strength of SAC signaling mediated by Knl1$^{\Delta}$-
242 M3 and Knl1$^{\Delta}$-M3-M3 specifically in GSK923295-treated cells. We used time-lapse imaging to
243 monitor mitotic progression in cells treated with different concentrations of GSK923295 to achieve
244 different degrees of CENP-E inhibition resulting in different durations of mitotic arrests. For all the
245 concentrations tested, cells expressing Knl1$^{\Delta}$-M3-M3 arrested for significantly longer durations
246 compared to cells expressing Knl1$^{\Delta}$-M3 (Figure 4A-B). The same trend was observed when these
247 cells were treated with Taxol (Figure 4C). Thus, the number of MELT motifs in Knl1 can determine
248 the duration of checkpoint-induced mitotic delays in cells wherein a few signaling kinetochores
249 sustain the SAC. When combined with the results described in the previous section, this finding
250 implies that the higher recruitment of Bub1, BubR1, and Mad1 per kinetochore is correlated with
251 longer delays in anaphase onset.

252

253 **Bub1 over-expression results in higher recruitment of SAC proteins to the kinetochore**

254 A significant fraction of MELT motifs in Knl1 are unoccupied in the GSK923295- and nocodazole-
255 treated cells (Vleugel et al., 2015; Zhang et al., 2014). Our data also suggest that Bub1 depletion
256 contributes to the lower-than-expected recruitment of SAC proteins. Therefore, we reasoned that
257 the unoccupied MELT motifs will be pressed into action if Bub1 is overexpressed.

258 We over-expressed mNG-Bub1 using a doxycycline-inducible promoter and quantified the
259 recruitment of Bub1, BubR1, and Mad1 per kinetochore in cells treated with GSK923295 using
260 immunofluorescence. As expected, mNG-Bub1 localization at signaling kinetochores was
261 detectable when following doxycycline treatment (micrographs in Figure 5A). To measure the total
262 amount of Bub1 per kinetochore, we fixed and stained these cells with anti-Bub1 antibodies
263 (Methods). Fluorescence quantification confirmed that signaling kinetochores in the doxycycline-
264 treated cells recruited ~35% more Bub1 than signaling kinetochores in untreated cells (Figure 5A,
265 plot on the left). Importantly, signaling kinetochores in the doxycycline-treated cells also recruited
266 26% more BubR1 (Figure 5A, middle plot). The amount of Mad1 per kinetochore did not change
267 (Figure 5A, right plot). Thus, signaling kinetochores in HeLa cells can recruit more Bub1 and
268 BubR1 if there is sufficient Bub1 is available. However, Mad1 recruitment does not increase likely
269 because of the low abundance of Mad1.

270

271 **Bub1 overexpression results in longer delays in SAC-mediated anaphase onset, but only**
272 **cells containing small numbers of signaling kinetochores**

273 To test whether Bub1 overexpression also results in longer delays in anaphase onset, we
274 released either untreated or doxycycline-treated cells from a G1/S block into media containing
275 18-35 nM GSK923295 and quantified the average time spent in mitosis in each case (Figure 5B,
276 Methods). We found that the doxycycline-treated cells arrested for ~ 145 min on average
277 compared to the untreated cells, which arrested for ~ 94 min (Figure 5B, left, also see
278 Supplementary Videos S1 and S2). To understand the correlation between the expression level
279 of exogenous Bub1 and the mitotic duration, we plotted the mitotic duration against the cellular
280 mNG signal in both cases (the fluorescence values were normalized to the average mNG
281 fluorescence per cell from samples not treated with doxycycline, 5B right). As expected, there
282 was no correlation between the cellular mNG signal and mitotic duration in the untreated cells
283 (gray circles, Pearson's correlation coefficient displayed at the top right of the figure). In contrast,

284 the mitotic duration of cells treated with doxycycline was positively correlated with the mNG-Bub1
285 signal (orange circles in Figure 5B).

286 We also examined whether Bub1 overexpression produces longer delays in anaphase onset in
287 nocodazole-treated cells (Figure 5C). Interestingly, the correlation between the cellular mNG
288 signal and the duration of mitosis was not significant in nocodazole-treated cells (Figure 5C). The
289 likely explanation for this observation is that even with increased Bub1 recruitment, the large
290 number of signaling kinetochores cannot recruit higher amounts of BubR1 because of its depletion
291 (implied by reduced BubR1 recruitment in the nocodazole-treated cells, Figure 1). Because
292 BubR1 recruitment to the kinetochore promotes SAC signaling activity (Banerjee et al., 2021), the
293 Bub1 overexpression cannot promote SAC signaling.

294 These results confirm that the cellular Bub1 abundance is an important determinant of its own
295 recruitment and that of BubR1 to signaling kinetochores. These findings are consistent with
296 results from budding yeast, wherein the low cellular abundance of Bub1 limits its recruitment, and
297 that of Mad1, to signaling kinetochores (Aravamudhan et al., 2016; Roy et al., 2020). Together
298 with our earlier results, this experiment shows that low Bub1 abundance limits the SAC signaling
299 activity of kinetochores in HeLa cells.

300

301 **Partial depletion of Bub1 and BubR1, but not Mad1, strongly reduces the duration of**
302 **mitosis in cells containing small numbers of unattached kinetochores**

303 Mad1 and Bub1 abundance in HeLa cells is similar (Banerjee et al., 2021), which suggests that
304 Mad1 availability will also put a limit on the maximal MCC production rate. To test this notion, we
305 adopted a different approach. Rather than over-expressing Mad1, we partially knocked it down
306 using an siRNA against mNeonGreen in the genome-edited cell line heterozygous for Mad1-
307 mNG, and then observed its effect on the duration of SAC-induced mitotic delays. We also
308 lowered Bub1 and BubR1 levels using the same strategy. This strategy was adopted for two
309 reasons. First, to increase Mad1 recruitment at kinetochores, Bub1 may also have to be over-
310 expressed alongside Mad1 to provide additional Mad1 binding sites. Second, Mad1 over-
311 expression can weaken the SAC by depleting the Mad2 pool available for MCC formation, which
312 would complicate data interpretation (Barnhart et al., 2011; Chen et al., 1999; Ryan et al., 2012).

313 To confirm that the mNG-labeled protein can be specifically depleted, we treated the three cell
314 lines with mNG siRNA for 48 hours and used immunoblotting to assess the levels of Bub1, BubR1,
315 and Mad1. As expected, the mNG-tagged protein was significantly depleted, whereas the

316 unlabeled protein was unaffected (Figure 6A). Thus, the mNG siRNA treatment specifically
317 depletes the mNG-labeled protein and, after ~ 48 hours, reduces overall protein level in the
318 heterozygous cells by at most 50%. To study the effect of a mild depletion of SAC protein on the
319 SAC signaling strength of the kinetochore, we treated the three cell lines with mNG siRNA for ~
320 24 hours and observed the effects of protein depletion on mitotic duration in GSK923295- and
321 nocodazole-treated cells. Quantification of mNG fluorescence signal from mitotic cells revealed
322 that the mNG siRNA treated resulted in an average reduction of ~ 50% in the level of the mNG-
323 labeled protein in all three cell lines (Figure 6B). Because only about half of the total protein is
324 labeled with mNG, this measured decrease corresponds to an average depletion of ~ 25% in each
325 case. The siRNA treatment also resulted in a significant decrease in mitotic duration in
326 GSK923295-treated cells (Figure 6C, left). Partial depletion of either Bub1 or BubR1 had a strong
327 effect: the average duration of mitosis decreased from ~ 1000 minutes to 300-500 minutes (Figure
328 6C). We also confirmed that the partial depletion of BubR1 in GSK923295-treated cells resulted
329 in chromosome missegregation (Supplementary Videos S3 and S4). Mad1 depletion has a
330 relatively minor effect on mitotic duration: the average time in mitosis decreased from ~ 1000
331 minutes to 868 minutes (Figure 6C). Interestingly, in nocodazole-treated cells, the partial
332 depletion of all three proteins did not significantly change the duration of mitosis (Figure 6C, right).

333 These data show that even a small (~ 25% on average) reduction in Bub1 or BubR1 level results
334 in a significant decrease in the duration of mitosis in GSK923295-treated cells, but not in
335 nocodazole-treated cells. However, a similar depletion of Mad1 levels results in a relatively lower
336 decrease in the duration of mitosis. Consistent with previous report, the partial depletion of Bub1
337 had a minor effect on the duration of mitosis in nocodazole-treated cells (Morrow et al., 2005).

338

339 **Discussion**

340 Our results show that the number of signaling kinetochores in a mitotic HeLa cell strongly affects
341 the recruitment of Bub1, BubR1, and Mad1 to signaling kinetochores: the recruitment of each
342 protein per kinetochore is significantly higher in cells containing a few signaling kinetochores (i.e.,
343 the GSK923295-treated cells) compared to cells that contain many signaling kinetochores (i.e.,
344 the nocodazole-treated cells). The main factor responsible for this difference is the depletion of
345 cytoplasmic Bub1 available for recruitment in cells containing many signaling kinetochores. The
346 lower recruitment of SAC proteins per kinetochore lowers the signaling strength of the kinetochore
347 as evidenced by the shorter duration of mitosis in the GSK923295-treated cells expressing Knl1$^{\Delta}$-
348 M3 as opposed to Knl1$^{\Delta}$-M3-M3. Conversely, Bub1 over-expression increases the recruitment of

Bub1 and BubR1, but not Mad1, and the increased recruitment results in a significant increase in the mitotic duration only in GSK923295-treated cells. Importantly, this increase is not seen in nocodazole-treated cells. This observation parallels the sensitivity of the SAC to partial depletion of Bub1 and BubR1, but not Mad1, only in GSK923295-treated cells. The differential sensitivity of the SAC arises likely because a small number of signaling kinetochores must sustain the SAC in the GSK923295-treated cells (Roy et al., 2020). Each kinetochore must recruit SAC proteins robustly and signal at the maximal rate to maintain the cumulative MCC amount high. In nocodazole-treated cells, however, the significantly larger number of signaling kinetochores can maintain a higher cumulative level of MCC despite individual kinetochores signaling at sub-maximal rates.

The limitation on protein recruitment at signaling kinetochores, partially due to low Bub1 protein levels, is a major factor behind the inverse correlation between the number of signaling kinetochores in a cell and the signaling strength of each kinetochore. Importantly, this correlation is not due to changes in the phosphoregulation of the kinetochore. The inverse scaling is likely to be biologically significant. Because of it, the many, concurrently signaling kinetochores following NEBD will not be able to generate MCC at a higher rate, but when the number of signaling kinetochores is low, the remaining kinetochores will signal more strongly to compensate for the lower number of signaling kinetochores. An interesting possibility is that synergistic signaling by the Knl1 phosphodomain under this condition will further strengthen the signaling activity of these remaining kinetochores (Chen et al., 2019).

Our results also raise important questions requiring further investigation. First, it remains unclear why kinetochores in HeLa cells and other eukaryotes use only a small fraction of their signaling strength. One possibility is that this modulation of the signaling strength of the kinetochore represents a compromise that balances SAC signaling strength with its responsiveness to silencing mechanisms (Roy et al., 2020). Higher Bub1 expression may also have drawbacks in other aspects of mitosis and cell biology, in which case its low expression level would represent a compromise between different cellular objectives. Finally, these results reveal how relatively small perturbations or imbalance in the expression level of Bub1 and other SAC proteins can contribute to the high rates of chromosome missegregation commonly observed in cancer cells.

382 **Acknowledgements**

383 This work was supported by R35-GM126983 from NIGMS to APJ. We thank Dr. Geert Kops for
384 kindly sharing the design details for the Mps1sen-Kt construct, Dr. Iain Cheeseman and Dr. Mara
385 Duncan for feedback on the manuscript and useful discussion.

386 **Materials and Methods**
387
388 **Cell culture**
389 Henrietta Lacks (HeLa) A12 cells (a kind gift from the Makeyev lab) were grown in DMEM media
390 supplemented with 10% FBS, 1% Pen-Strep, 25 mM HEPES buffer, and 1x Gluta-max at 37 °C
391 and 5% CO2. Antibiotics used: 1-2 µg/ml Puromycin or 1 µg/ml Blasticidin as needed. To express
392 recombinant proteins, we modified a bicistronic vector designed by the Makeyev lab as necessary
393 (Khandelia et al., 2011). The modified vectors were transfected into HeLa A12 cells that have the
394 *Loxp*-Blasticidin-*Lox2272* cassette engineered into their genome. Transformed cells were pooled
395 and used for further experimentation. The construction of genome-edited HeLa A12 cell lines has
396 been described in detail previously (Chen et al., 2019). The methodology used to construct the
397 genome-edited HeLa A12 cell lines has been described in detail in (Banerjee et al., 2021). A
398 revised version of this related manuscript is included as a supplementary data file.
399
400 Imaging experiments were performed in Fluorobrite media supplemented with FBS, Pen-Strep,
401 HEPES as noted above. G1/S synchronization was achieved using a 2-thymidine block (2.5 mM
402 Thymidine). On the day of imaging, cells were released from the second block and treated with
403 either 330 nM nocodazole or 236 nM GSK923295 ~ 1.5 hour prior to imaging.
404
405 **Immunoblotting**
406 To acquire unsynchronized HeLa-A12 cells, cells were either scrapped or trypsinized off the
407 surface of dishes. To acquired mitotic HeLa-A12 cells, cells were first synchronized in G1/S with
408 2.5mM thymidine and then arrested in mitosis with 330nM of nocodazole for 16h before mitotic
409 shake-off. Shook- off mitotic cells were then washed once by phosphate-buffered saline (Gibco),
410 pelleted down, and chilled on ice. Lysis was performed by directly adding 2x Laemmli sample
411 buffer (supplemented by 2-mercaptoethanol, Bio-Rad Laboratories) at a ratio of 1µL per 0.1mg of
412 cell pellets and pipetting up and down. Lysates were boiled immediately afterward for 10min and
413 then chilled on ice. 8µL of supernatant was loaded onto each lane of a 15-well, 0.75-mm SDS-
414 PAGE mini gel.
415 Primary antibodies used included antiBUBR1 (Bethyl Laboratories A300-995A, 1 : 1000), anti-
416 MAD1 (GeneTex GTX109519, 1 : 2000), anti-CDC20 (Santa Cruz Biotechnology sc-13162, 1 :
417 200), anti-BUB3 (Sigma-Aldrich B7811, 1 : 500), anti-mNeonGreen (ChromoTek 32F6, 1 : 500),
418 anti-GAPDH (Proteintech 60004-1-Ig, 1 : 5000), anti-BUB1 (three antibodies purified from different
419 hosts were used: (1) Bethyl Laboratories A300-373A, 1 : 330, rabbit polyclonal antibody; (2) SB1.3

420 [55], 1 : 1000, sheep polyclonal antibody; (3) Abcam ab54893, 1 : 200, mouse monoclonal
421 antibody), and anti-DsRed2 (Santa Cruz Biotechnology sc101526, 1 : 5000).

422

423 **RNA interference**

424 Cells were transfected with siRNA in the morning. 2.5 mM of thymidine was added 8 h later and
425 cells were incubated overnight. The next morning, cells were released from the thymidine block
426 into fresh media. This sequence was then repeated once again and cells were released into
427 FluoroBrite™ DMEM (Gibco) supplemented with 9% (by volume) of fetal bovine serum and 1x
428 GlutaMAX and incubated for 6 h before the addition of mitotic drugs. Drugs were left to take effect
429 for 1 h before imaging.

430 Sense-strand sequences and working concentrations of small interfering RNA duplexes (siRNAs)
431 used in this study include the *BUBR1* siRNA (5'-GAUGGUGAAUUGUGGAAUA-3', 40 nM [96]),
432 *BUB1* siRNA (5'-CGAAGAGUGAUCACGAUUU-3', 40 nM [97]), and the *ZW10* siRNA (5'-
433 UGAUCAAUGUGCUGUUCAA-3', 100 nM [62]). The siRNAs against all five B56 isoforms were
434 taken from the second pool in [98]. Desalted siRNA duplexes modified by double-deoxythymidine
435 overhangs at 3'-ends of both strands were synthesized by Sigma. The AllStar Negative Control
436 siRNA (QIAGEN) was used as the control. All siRNAs were transfected into the cells via
437 Lipofectamine RNAiMAX (Invitrogen) following manufacturer's instructions.

438

439 **Live-cell imaging**

440 Cells were plated in a Nunc Lab-Tek II chambered cover glass (Thermo Scientific) or a 35mm
441 cover glass-bottomed dish (MatTek) and treated with drugs and/or siRNAs as described above.
442 For imaging, the chambered cover glass or the cover glass-bottomed dish was loaded into a CU-
443 501 temperature and gas control system (Live Cell Instrument). The sample holder was
444 maintained at 37°C and ventilated by humidified 5% of CO_2 and the objective was maintained at
445 37°C by a heating band.

446 With the exception of MPS1sen-KT FRET measurements, imaging was performed on a Nikon
447 Eclipse Ti-E/B inverted microscope, with a CFI Plan Apochromat Lambda 100x, 1.45 NA oil
448 objective (Nikon). The microscope was equipped with an H117E1 motorized stage (Prior
449 Scientific) and a NanoScanZ 100 piezo stage (Prior Scientific). A SPECTRA 5-LCR-XA Light
450 Engine (Lumencor) served as the excitation light source. The 475 nm-centered band of excitation
451 light was used for the green channel and the 575/30nm-filtered band of excitation light was used

452 for the red channel. An ET-EGFP/mCherry filter cube (Chroma Technology) was used as the
453 dichroic mirror, where the built-in emission filter on the cube has been removed. Emission light in
454 the red channel was filtered by an ET632/60m (Chroma Technology). Emission light in the green
455 channel was filtered by an ET525/50m (Chroma Technology). Emission filters were mounted on
456 a high-speed filter wheel (Prior Scientific) positioned in the light path. Images were acquired with
457 a iXon3 EMCCD camera (Andor Technology) operating in the conventional CCD mode. Signaling
458 kinetochores in GSK923295-treated cells were identified by their polar positioning and the
459 enrichment of localized SAC proteins on them.

460 The FRET measurement with MPS1sen-KT was also performed on a Nikon Eclipse TiE/B inverted
461 microscope, with a CFI Plan Apochromat VC 100x, 1.40 NA oil objective (Nikon). The microscope
462 was equipped with an H117E1 motorized stage (Prior Scientific), a NanoScanZ 100 piezo stage
463 (Prior Scientific), and an X-Light V2 L-FOV confocal unit with 60μm pinholes (CrestOptics). A
464 CELESTA Light Engine (Lumencor) served as the excitation laser source. The 477-nm line (at
465 25% power with an exposure time of 400ms for each frame) was used for both the green and the
466 FRET channels and the 546-nm line (at 50% power with an exposure time of 400ms for each
467 frame) was used for the red channel. A ZT488/543rpc (Chroma Technology) was used as the
468 dichroic mirror. Emission through both the red and the FRET channels was filtered by an
469 ET605/52m (Chroma Technology) while emission through the green channel was filtered by an
470 ET525/36m (Chroma Technology). Images were acquired by a Prime 95B 25mm sCMOS camera
471 (Teledyne Photometrics). Custom MATLAB programs [99] were used to quantify kinetochore-
472 localized fluorescence signals.

473 Time-lapse live-cell imaging related to the knockdown-rescue experiments was performed on an
474 ImageXpress Nano Automated Imaging System (Molecular Devices). A SOLA Light Engine
475 (Lumencor) served as the excitation light source. Cells were plated on 24-well cell imaging plates
476 (black plate with treated glass bottom, Eppendorf) and treated with drugs and/or siRNAs
477 accordingly. Input humidified 5% CO_2 flow was maintained at around 19psi and the environment
478 chamber was maintained at 37°C. All SAC proteins tagged by mNeonGreen in this chapter
479 (BUBR1, BUB1, and MAD1) feature inhomogeneous distributions between the cytosol and the
480 nucleus/nuclear envelope in the prophase (data not shown). In principle, they can indicate the
481 accurate timing of the nuclear envelope breakdown (NEBD) in each cell during the time-lapse
482 imaging. However, due to the resolution limit and for consistency, we determined mitotic duration
483 mainly based on cell morphology (from rounding-up at the NEBD to elongation at the anaphase

484 onset) from transmitted-light images. This was facilitated by the semi-automatic image analysis
485 pipeline described in Section 2.3.

486

487 **Immunofluorescence**

488 Hela cells that exogenously expressing mNG-Bub1 were plated on a 12mm coverslip and
489 synchronized by Thymidine (2.5 mM for 8 hours) followed by RO3306 treatment (15 nM for 20
490 hr). G2/M arrested cells were washed three times with PBS and released into media containing
491 GSK923235 (23.6 nM) for 4 hours) to get arrested in Mitosis. For immunolabeling, the cells were
492 pre-extracted with 0.5% Triton X-100 in 0.1 M PHEM (240 mM Pipes, 100 mM HEPES, 8 mM
493 MgCl2 and 40 mM EGTA) and then fixed with 4% PFA for 10 min. The coverslips were washed
494 three times with 0.1 M PHEM buffer and blocked for 30 min at room-temperature with 5% Donkey
495 serum. Next, the coverslips were incubated in anti-Mad1 (1:1000, Sigma M80691), anti-Bub1
496 (1:500, Thermo A300-373A), or anti-BubR1 (1:1000, Thermo Scientific A300-373A) over night at
497 4°C. The next day, the coverslips were washed 4 times with 1xPHEM containing 0.05% Tween-
498 20 and incubated with appropriate secondary antibodies (1:10000 Goat anti-Mouse633,
499 Invitrogen A21052, 1:10000 Goat anti-Rabbit633, Invitrogen A21071) for 45 min at room
500 temperature in the dark. Following secondary antibody labeling, the coverslips were washed four
501 times and mounted in antifade solution (ProLong; Molecular Probes).

502 Immunofluorescence images were taken on a Nikon inverted microscope equipped with a Crest
503 X-Light V2 LFOV25 Spinning Disk Confocal head, and Photometric 95B Prime cMOS camera.
504 For each field of view, 31 Z sections were acquired at 0.2 mm steps using a 100x, 1.4 Numerical
505 Aperture (NA) Nikon objective.

506

507 **Fluorescence correlation spectroscopy (FCS)**

508 The total number of fluorophores in a homogeneous solution is $N_{total} := N_A c V_{total}$, where N_A is the
509 Avogadro constant, c is the molar concentration of the fluorophore, and V_{total} is the total volume
510 of the solution. The probability that a specific fluorophore molecule is within the excitation volume
511 $V_0 (\ll V_{total})$ at any given time is $p_0 := V_0/V_{total} \ll 1$. For freely diffusive fluorophores in a diluted
512 solution, whether or not a specific fluorophore is within the excitation volume is independent of
513 each other. Thus, the number of fluorophores inside the excitation volume at any given time N_0
514 has a binomial distribution $B(N_{total}, p_0)$. Therefore,

515 $$G_0 := \frac{\sigma_{N_0}^2}{\langle N_0 \rangle^2} = \frac{1}{N_{\text{total}} p_0} \frac{p_0}{} \approx \frac{1}{N_{\text{A}} c V_0}$$

516 Under a fixed live-cell imaging setup [which includes the microscope (its alignment and the
517 objective), the wavelength of the excitation light, the thickness of the coverslip (affecting the actual
518 working distance), and the refractive index of the cytosol], V_0 is fixed. Therefore, G_0 is inversely
519 proportional to the molar concentration of the fluorophore. The average number (or the variance
520 of the number) of fluorophores inside the excitation volume observed over a long period should
521 be close to the theoretical mean $\langle N_0 \rangle$ (or the theoretical variance σ^2_{N0}).

522 All FCS data were collected on an Alba v5 Laser Scanning Microscope (ISS), connected to an
523 Olympus IX81 inverted microscope main body [equipped with a UPLSAPO60XW objective (1.2
524 NA, Olympus)]. A Fianium WL-SC-400-8 laser (NKT Photonics) with an acoustooptic tunable filter
525 was used to generate excitation pulses at a wavelength of 488nm and a frequency of around
526 20MHz. Excitation light was further filtered by a Z405/488/561/635rpc quadband dichroic mirror
527 (Chroma). Emission went through a 655DCSPXR short-pass dichroic mirror (Chroma) and an
528 FF01-531/40-25 filter (Semrock) and was finally detected by an SPCM-AQRH-15 avalanche
529 photodiode (Perkin Elmer). The time-correlated single photon counting module to register
530 detected photon events to excitation pulses was SPC830 (Becker & Hickl). Data acquisition was
531 facilitated by VistaVision (ISS). The excitation volume (V_0) was calibrated by taking FCS data from
532 TetraSpeck™ microspheres (0.1µm, Invitrogen) of known concentrations (vary across different
533 batches).

534

535 **Quantification of the FRET based on localized fluorescence signals of MPS1sen-KT**

536 Under fixed fluorescence microscopy settings of a given channel (the excitation line and its power,
537 exposure time, optical components including the objective, filters, dichroic mirrors, the confocal
538 spinning disk, and the detector in the light path and their alignment, etc.), the kinetochore-localized
539 fluorescence signal (digital readout) should be proportional to the number of localized mature
540 fluorescence proteins. The coefficients are designated as g and r_x for mNeonGreen and mScarlet-
541 I using the excitation light for mNeonGreen, respectively (the subscript "x" stands for cross-
542 excitation as mScarlet-I is excited by the excitation light for mNeonGreen here). The number of
543 unbleached mature mNeonGreen and mScarlet-I molecules at a given kinetochore are G and R,
544 respectively. While measuring FRET using the excitation light for mNeonGreen and optics
545 settings to detect the emission of mScarlet-I, the bleed-through coefficient for mNeonGreen

fluorescence is designated as . Under a FRET efficiency of ε ($0 \leq \varepsilon \leq 1$, which describes the quenching of mNeonGreen due to FRET), the proximity ratio Θ, a metric of FRET according to the definition in [99], can be expressed as:

$$\Theta = \frac{\mathrm{F}}{\mathrm{r}_x R + \beta g G(1-\varepsilon)} - 1$$

where *F* is the measured raw FRET readout. *F* can be attributed to three sources: (1) the cross-excitation of mScarlet-I, (2) the bleed-through of mNeonGreen fluorescence, and (3) the actual fluorescence due to FRET (determined by the combined coefficient *f* for the excited fraction of mNeonGreen under the excitation condition of the FRET channel and the conversion from FRET emission photons reaching the detector to the digital readout, the FRET efficiency, and the effective quantum yield of mScarlet-I that reaches the detector).

$$F = r_x R + \beta g G(1-\varepsilon) + f G \varepsilon \phi$$

In [64], the authors used the ratio between the mNeonGreen signal (measured from the green channel) and the raw FRET signal (without corrections of the cross-excitation of mScarlet-I and the bleed-through of mNeonGreen's fluorescence) as the metric of FRET:

$$\Gamma = \frac{\mathrm{gG}(1-\varepsilon)}{\mathrm{F}}$$

Because MPS1sen-KT competes with endogenous SPC24 to get recruited to the outer kinetochore region, the number of kinetochore-localized sensors is variable for different kinetochores. However, the ratio between kinetochore-localized mNeonGreen and mScarlet-I is always 1 : 1. Ignoring photobleaching (only one *z*-stack is taken for each cell with a bare minimum amount of exposure) and assuming that maturation of mNeonGreen and mScarlet-I is independent of the kinases' or phosphatases' activity at kinetochores, σ:= *R/G* should also be fixed. Hence, we have:

$$\Theta = \frac{\mathrm{f}\varepsilon\phi}{\mathrm{r}_x \sigma + \beta g G(1-\varepsilon)}$$

$$x = \frac{g(1-\varepsilon)}{\mathrm{r}_x \sigma + \beta g(1-\varepsilon) + f\varepsilon\phi}$$

Importantly, both Θ and Γ are dimensionless metrics normalized against the variation in the kinetochore localization of MPS1sen-KT. Under a particular fluorescence microscopy setting, both Θ and Γ have a monotonic and hyperbolic relationship with the FRET efficiency and are interconvertible:

$$\Theta = \frac{g(1-\varepsilon)}{\mathrm{r}_x\sigma + \beta g(1-\varepsilon)} \cdot \frac{1}{\Gamma} - 1$$

Statistical analysis

Statistical analysis was conducted using GraphPad Prism version 8.

580 **References**

581 Aravamudhan, P., Chen, R., Roy, B., Sim, J., and Joglekar, A.P. (2016). Dual mechanisms regulate
582 the recruitment of spindle assembly checkpoint proteins to the budding yeast kinetochore. Mol
583 Biol Cell *27*, 3405-3417.
584 Banerjee, A., Chen, C., Humphrey, L., Tyson, J.J., and Joglekar, A.P. (2021). BubR1 recruitment to
585 the kinetochore via Bub1 enhances Spindle Assembly Checkpoint signaling. bioRxiv,
586 2021.2008.2012.456107.
587 Barnhart, E.L., Dorer, R.K., Murray, A.W., and Schuyler, S.C. (2011). Reduced Mad2 expression
588 keeps relaxed kinetochores from arresting budding yeast in mitosis. Mol Biol Cell *22*, 2448-2457.
589 Chen, C., Whitney, I.P., Banerjee, A., Sacristan, C., Sekhri, P., Kern, D.M., Fontan, A., Kops, G.,
590 Tyson, J.J., Cheeseman, I.M.*, et al.* (2019). Ectopic Activation of the Spindle Assembly Checkpoint
591 Signaling Cascade Reveals Its Biochemical Design. Curr Biol *29*, 104-119 e110.
592 Chen, R.-H., Brady, D.M., Smith, D., Murray, A.W., and Hardwick, K.G. (1999). The Spindle
593 Checkpoint of Budding Yeast Depends on a Tight Complex between the Mad1 and Mad2 Proteins.
594 Molecular Biology of the Cell *10*, 2607-2618.
595 Clute, P., and Pines, J. (1999). Temporal and spatial control of cyclin B1 destruction in metaphase.
596 Nat Cell Biol *1*, 82-87.
597 Collin, P., Nashchekina, O., Walker, R., and Pines, J. (2013). The spindle assembly checkpoint
598 works like a rheostat rather than a toggle switch. Nat Cell Biol *15*, 1378-1385.
599 Dick, A.E., and Gerlich, D.W. (2013). Kinetic framework of spindle assembly checkpoint signalling.
600 Nat Cell Biol *15*, 1370-1377.
601 Faesen, A.C., Thanasoula, M., Maffini, S., Breit, C., Muller, F., van Gerwen, S., Bange, T., and
602 Musacchio, A. (2017). Basis of catalytic assembly of the mitotic checkpoint complex. Nature.
603 Izawa, D., and Pines, J. (2015). The mitotic checkpoint complex binds a second CDC20 to inhibit
604 active APC/C. Nature *517*, 631-634.
605 Ji, Z., Gao, H., Jia, L., Li, B., and Yu, H. (2017). A sequential multi-target Mps1 phosphorylation
606 cascade promotes spindle checkpoint signaling. Elife *6*.
607 Khandelia, P., Yap, K., and Makeyev, E.V. (2011). Streamlined platform for short hairpin RNA
608 interference and transgenesis in cultured mammalian cells. Proc Natl Acad Sci USA *108*, 12799-
609 12804.
610 Kops, G.J., Kim, Y., Weaver, B.A., Mao, Y., McLeod, I., Yates, J.R., 3rd, Tagaya, M., and Cleveland,
611 D.W. (2005). ZW10 links mitotic checkpoint signaling to the structural kinetochore. J Cell Biol *169*,
612 49-60.
613 Krefman, N.I., Drubin, D.G., and Barnes, G. (2015). Control of the spindle checkpoint by lateral
614 kinetochore attachment and limited Mad1 recruitment. Mol Biol Cell.
615 Kuhn, J., and Dumont, S. (2019). Mammalian kinetochores count attached microtubules in a
616 sensitive and switch-like manner. J Cell Biol *218*, 3583-3596.
617 Kuijt, T.E.F., Lambers, M.L.A., Weterings, S., Ponsioen, B., Bolhaqueiro, A.C.F., Staijen, D.H.M.,
618 and Kops, G. (2020). A Biosensor for the Mitotic Kinase MPS1 Reveals Spatiotemporal Activity
619 Dynamics and Regulation. Curr Biol *30*, 3862-3870 e3866.
620 Lara-Gonzalez, P., Kim, T., Oegema, K., Corbett, K., and Desai, A. (2021a). A tripartite mechanism
621 catalyzes Mad2-Cdc20 assembly at unattached kinetochores. Science *371*, 64-67.

622 Lara-Gonzalez, P., Pines, J., and Desai, A. (2021b). Spindle assembly checkpoint activation and
623 silencing at kinetochores. Semin Cell Dev Biol *117*, 86-98.
624 London, N., and Biggins, S. (2014). Mad1 kinetochore recruitment by Mps1-mediated
625 phosphorylation of Bub1 signals the spindle checkpoint. Genes Dev *28*, 140-152.
626 London, N., Ceto, S., Ranish, J.A., and Biggins, S. (2012). Phosphoregulation of Spc105 by Mps1
627 and PP1 regulates Bub1 localization to kinetochores. Curr Biol *22*, 900-906.
628 Mapelli, M., Massimiliano, L., Santaguida, S., and Musacchio, A. (2007). The Mad2 conformational
629 dimer: structure and implications for the spindle assembly checkpoint. Cell *131*, 730-743.
630 Morrow, C.J., Tighe, A., Johnson, V.L., Scott, M.I., Ditchfield, C., and Taylor, S.S. (2005). Bub1 and
631 aurora B cooperate to maintain BubR1-mediated inhibition of APC/CCdc20. J Cell Sci *118*, 3639-
632 3652.
633 Musacchio, A. (2015). The Molecular Biology of Spindle Assembly Checkpoint Signaling Dynamics.
634 Curr Biol *25*, R1002-1018.
635 Pereira, C., Reis, R.M., Gama, J.B., Celestino, R., Cheerambathur, D.K., Carvalho, A.X., and
636 Gassmann, R. (2018). Self-Assembly of the RZZ Complex into Filaments Drives Kinetochore
637 Expansion in the Absence of Microtubule Attachment. Curr Biol *28*, 3408-3421 e3408.
638 Piano, V., Alex, A., Stege, P., Maffini, S., Stoppiello, G.A., Huis In 't Veld, P.J., Vetter, I.R., and
639 Musacchio, A. (2021). CDC20 assists its catalytic incorporation in the mitotic checkpoint complex.
640 Science *371*, 67-71.
641 Primorac, I., Weir, J.R., Chiroli, E., Gross, F., Hoffmann, I., van Gerwen, S., Ciliberto, A., and
642 Musacchio, A. (2013). Bub3 reads phosphorylated MELT repeats to promote spindle assembly
643 checkpoint signaling. Elife *2*, e01030.
644 Qian, X., McDonald, A., Zhou, H.J., Adams, N.D., Parrish, C.A., Duffy, K.J., Fitch, D.M., Tedesco, R.,
645 Ashcraft, L.W., Yao, B.*, et al.* (2010). Discovery of the First Potent and Selective Inhibitor of
646 Centromere-Associated Protein E: GSK923295. ACS Med Chem Lett *1*, 30-34.
647 Rodriguez-Rodriguez, J.A., Lewis, C., McKinley, K.L., Sikirzhytski, V., Corona, J., Maciejowski, J.,
648 Khodjakov, A., Cheeseman, I.M., and Jallepalli, P.V. (2018). Distinct Roles of RZZ and Bub1-KNL1
649 in Mitotic Checkpoint Signaling and Kinetochore Expansion. Curr Biol *28*, 3422-3429 e3425.
650 Roy, B., Han, S.J.Y., Fontan, A.N., Jema, S., and Joglekar, A.P. (2022). Aurora B phosphorylates
651 Bub1 to promote spindle assembly checkpoint signaling. Curr Biol *32*, 237-247 e236.
652 Roy, B., Han, S.J.Y., Fontan, A.N., and Joglekar, A.P. (2020). The copy-number and varied strength
653 of MELT motifs in Spc105 balance the strength and responsiveness of the Spindle Assembly
654 Checkpoint. Elife *9*.
655 Ryan, S.D., Britigan, E.M., Zasadil, L.M., Witte, K., Audhya, A., Roopra, A., and Weaver, B.A. (2012).
656 Up-regulation of the mitotic checkpoint component Mad1 causes chromosomal instability and
657 resistance to microtubule poisons. Proc Natl Acad Sci USA *109*, E2205-2214.
658 Sacristan, C., Ahmad, M.U.D., Keller, J., Fermie, J., Groenewold, V., Tromer, E., Fish, A., Melero,
659 R., Carazo, J.M., Klumperman, J.*, et al.* (2018). Dynamic kinetochore size regulation promotes
660 microtubule capture and chromosome biorientation in mitosis. Nat Cell Biol *20*, 800-810.
661 Shaner, N.C., Lambert, G.G., Chammas, A., Ni, Y., Cranfill, P.J., Baird, M.A., Sell, B.R., Allen, J.R.,
662 Day, R.N., Israelsson, M.*, et al.* (2013). A bright monomeric green fluorescent protein derived
663 from Branchiostoma lanceolatum. Nat Methods *10*, 407-409.

664 Shepperd, L.A., Meadows, J.C., Sochaj, A.M., Lancaster, T.C., Zou, J., Buttrick, G.J., Rappsilber, J.,
665 Hardwick, K.G., and Millar, J.B. (2012). Phosphodependent recruitment of Bub1 and Bub3 to
666 Spc7/KNL1 by Mph1 kinase maintains the spindle checkpoint. Curr Biol *22*, 891-899.
667 Silio, V., McAinsh, A.D., and Millar, J.B. (2015). KNL1-Bubs and RZZ Provide Two Separable
668 Pathways for Checkpoint Activation at Human Kinetochores. Dev Cell *35*, 600-613.
669 Sudakin, V., Chan, G.K., and Yen, T.J. (2001). Checkpoint inhibition of the APC/C in HeLa cells is
670 mediated by a complex of BUBR1, BUB3, CDC20, and MAD2. J Cell Biol *154*, 925-936.
671 Suzuki, A., Badger, B.L., and Salmon, E.D. (2015). A quantitative description of Ndc80 complex
672 linkage to human kinetochores. Nat Commun *6*, 8161.
673 Tromer, E., Snel, B., and Kops, G.J. (2015). Widespread Recurrent Patterns of Rapid Repeat
674 Evolution in the Kinetochore Scaffold KNL1. Genome Biol Evol *7*, 2383-2393.
675 Vleugel, M., Omerzu, M., Groenewold, V., Hadders, M.A., Lens, S.M., and Kops, G.J. (2015).
676 Sequential multisite phospho-regulation of KNL1-BUB3 interfaces at mitotic kinetochores. Mol
677 Cell *57*, 824-835.
678 Vleugel, M., Tromer, E., Omerzu, M., Groenewold, V., Nijenhuis, W., Snel, B., and Kops, G.J.
679 (2013). Arrayed BUB recruitment modules in the kinetochore scaffold KNL1 promote accurate
680 chromosome segregation. J Cell Biol *203*, 943-955.
681 Zhang, G., Lischetti, T., Hayward, D.G., and Nilsson, J. (2015). Distinct domains in Bub1 localize
682 RZZ and BubR1 to kinetochores to regulate the checkpoint. Nat Commun *6*, 7162.
683 Zhang, G., Lischetti, T., and Nilsson, J. (2014). A minimal number of MELT repeats supports all the
684 functions of KNL1 in chromosome segregation. J Cell Sci *127*, 871-884.
685 Zhang, G., Mendez, B.L., Sedgwick, G.G., and Nilsson, J. (2016). Two functionally distinct
686 kinetochore pools of BubR1 ensure accurate chromosome segregation. Nat Commun *7*, 12256.
687

688 **Figure 1**

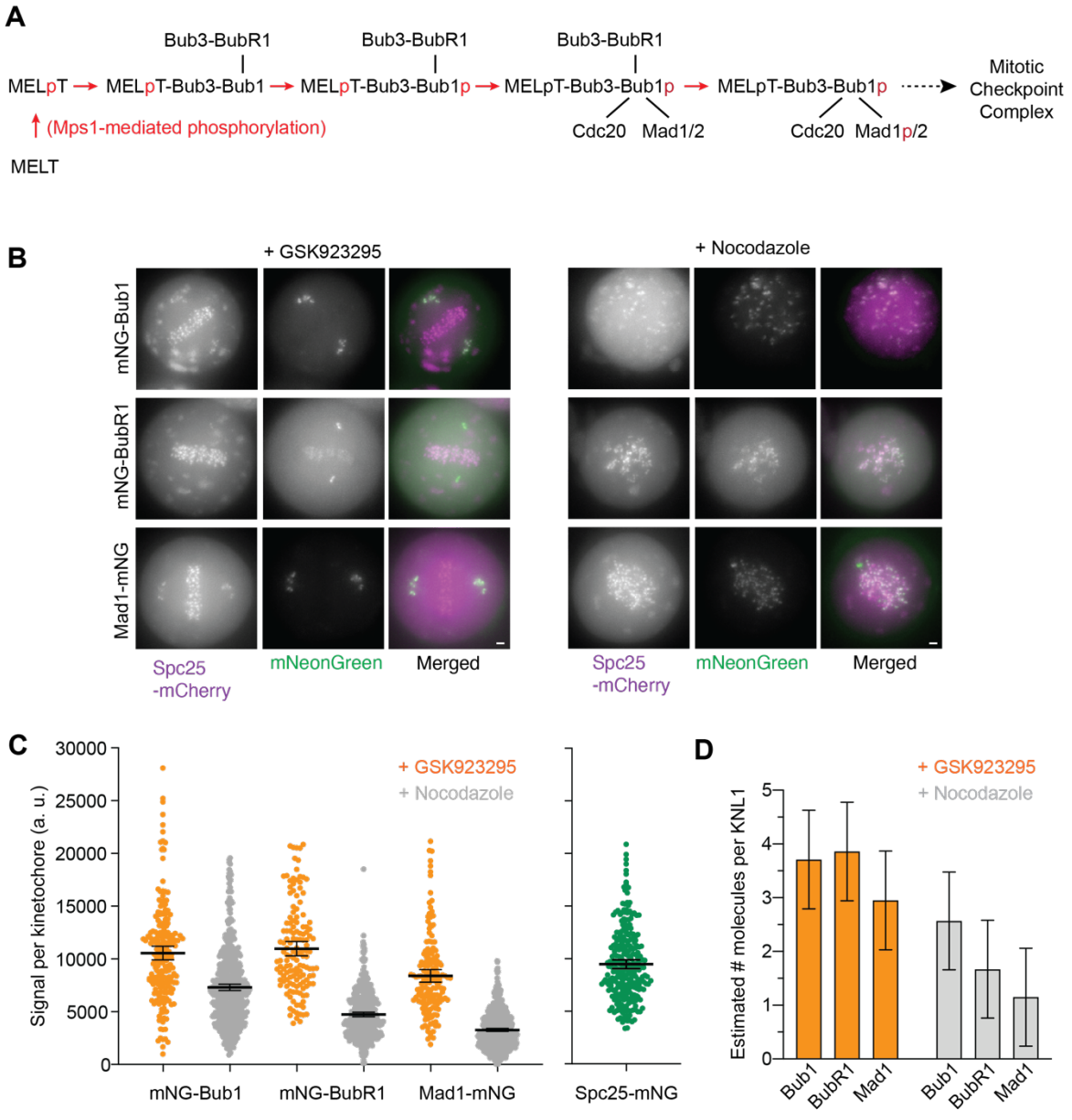

689

690

691 **Figure 1 Copy number of SAC proteins per kinetochore in mitotic cells containing different**
692 **numbers of signaling kinetochores.**

693 **(A)** A simplified schematic of the MELT motif-mediated recruitment of SAC proteins to the
694 kinetochore. Red arrows signify Mps1-mediated phosphorylation, black lines indicate
695 protein-protein interactions. The RZZ pathway, which is activated by Bub1 (Rodriguez-
696 Rodriguez et al., 2018; Sacristan et al., 2018; Zhang et al., 2015), is not shown.

697 **(B)** Representative fluorescence micrographs of mitotic HeLa cells expressing the indicated
698 proteins treated with GSK923295 (left) and nocodazole (right; scale bar ~ 1.6 μm)
699 **(C)** Quantification of the fluorescence signal per signaling kinetochore. Horizontal lines display
700 mean ± 95% confidence intervals (n = 200, 142, 160 in GSK923295-treated cells and 562,
701 446, and 658 in nocodazole-treated cells for Bub1, BubR1, and Mad1 respectively,
702 observations pooled from ≥ 2 technical repeats, $p < 0.0001$ for all three pairs of
703 measurements from Welch's t-test). Right: Spc25-mNG signal per kinetochore quantified
704 from images acquired under identical imaging conditions (n = 178).
705 **(D)** The estimated number of molecules per Knl1 calculated by dividing the mean signal per
706 kinetochore for each protein with the mean Spc25-mNG signal per kinetochore as the
707 reference. Error bars represent SEM for the calculated ratio.
708
709
710
711
712
713
714
715
716
717
718
719
720
721
722

723 **Figure 2**

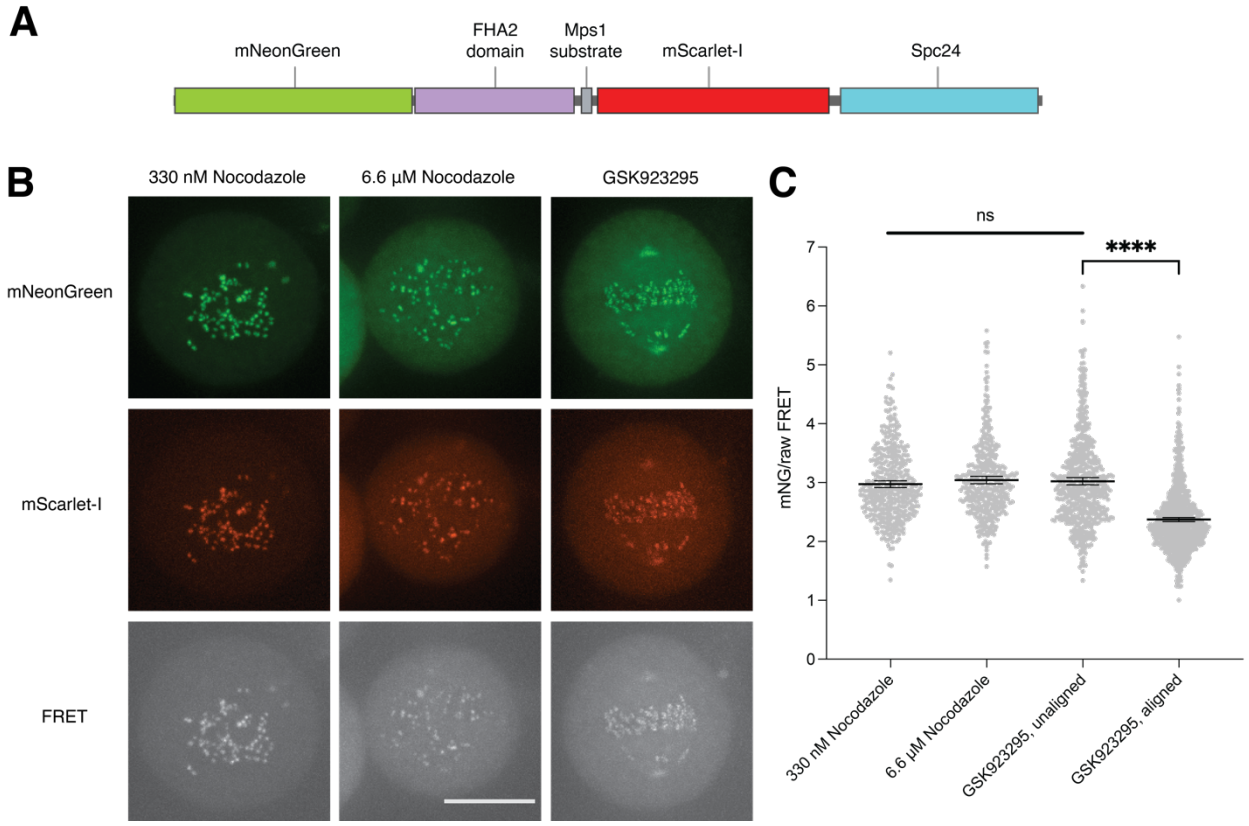

724

725 **Figure 2 Quantification of the Mps1-mediated phosphoregulation of signaling**
726 **kinetochores.**

727 **(A)** The modified design of MPS1sen-KT (Kuijt et al., 2020) wherein mNeonGreen/mScarlet-I is
728 used as the.

729 **(B)** Representative images of cells expressing MPS1sen-KT. The look-up table for each channel
730 (row) is universal for different groups (column). Scale bar, 10 µm.

731 **(C)** A summary of a normalized FRET metric (mNeonGreen signal/FRET signal) in HeLa A12
732 cells treated with different drugs at various concentrations. Each gray dot represents a single
733 kinetochore measurement. Data were compiled from at least two independent experiments (more
734 than 40 cells in total for each group). Mean values ± 95% confidence intervals are overlaid. Data
735 from cells treated with 45 nM, 90 nM, and 200 nM GSK923295 were pooled together (the mean
736 values are not significantly different from one another) to simplify the presentation. The Welch's
737 ANOVA test [W(DFn,DFd) = 1 .339(2.000,917.0), P= 0.2626] was performed for the first 3
738 columns (unaligned, signaling kinetochores). The unpaired t-test with Welch's correction
739 (P<0.0001) was performed to compare aligned non-signaling kinetochores with unaligned
740 signaling kinetochores in GSK923295-treated cells.

741

742 **Figure 3**

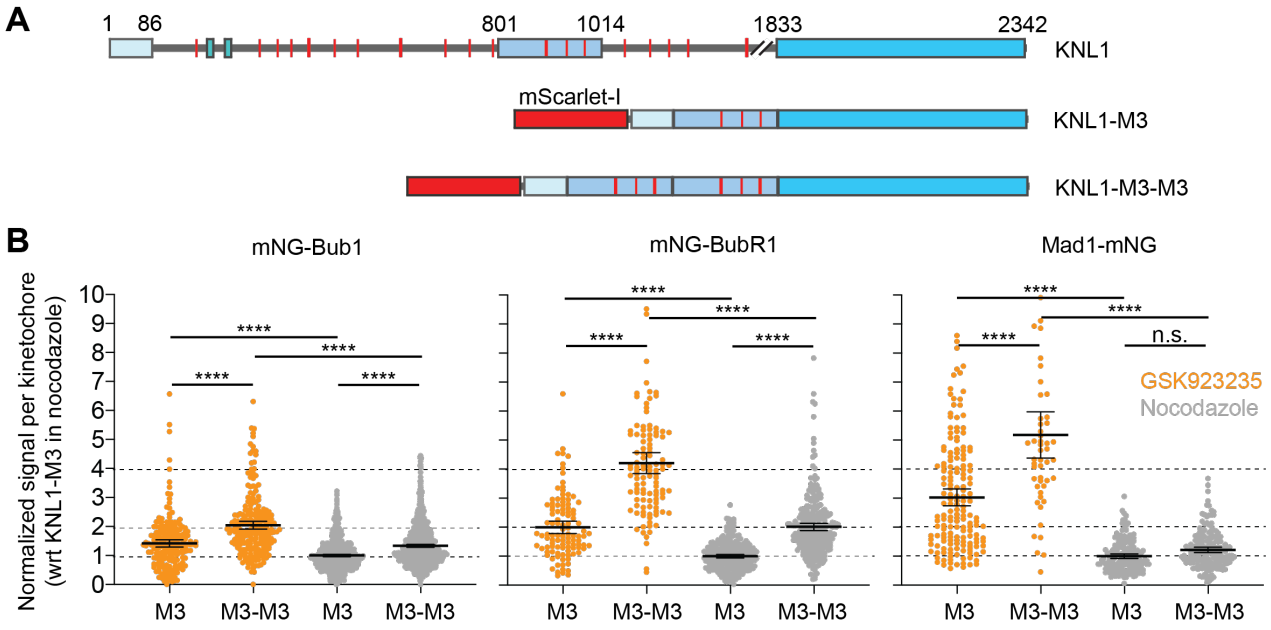

743

744 **Figure 3 – Copy number of SAC proteins per Knl1$^{\Delta}$-M3 and Knl1$^{\Delta}$-M3-M3 in cells containing**
745 **different numbers of signaling kinetochores.**

746 **(A)** Schematics of the full-length, endogenous Knl1 and the recombinant Knl1$^{\Delta}$-M3 and Knl1$^{\Delta}$-M3-
747 M3 versions. The expression of Knl1$^{\Delta}$-M3 (or Knl1$^{\Delta}$-M3-M3) is under the regulation of a
748 constitutive *EF1a* promoter. Therefore, Knl1$^{\Delta}$-M3 (or Knl1$^{\Delta}$-M3-M3) is always present in the
749 stably transfected cells.

750 **(B)** Quantification of the fluorescence signal per unaligned/laterally attached kinetochore for the
751 indicated protein. In each case, the signals were normalized using the mean signal for each
752 protein measured in nocodazole-treated cells (mNG-Bub1: n =844 and 602 for Knl1$^{\Delta}$-M3-M3
753 and Knl1$^{\Delta}$-M3 respectively in nocodazole-treated cells and 222 and 120 for Knl1$^{\Delta}$-M3-M3 and
754 Knl1$^{\Delta}$-M3 respectively in GSK923295-treated cells, pooled from ≥ 2 technical repeats; mNG-
755 BubR1: n = 278 and 272 in nocodazole-treated cells and 110 and 107 in GSK923295-treated
756 cells, pooled from ≥ 2 technical repeats; Mad1-mNG: n = 182 and 184 for Knl1$^{\Delta}$-M3-M3 and
757 Knl1$^{\Delta}$-M3 respectively in nocodazole-treated cells and 52 and 166 for Knl1$^{\Delta}$-M3-M3 and Knl1$^{\Delta}$-
758 M3 respectively in GSK923295-treated cells, pooled from ≥ 2 technical repeats). **** equivalent to p-value < 0.0001 according to one-way ANOVA.

760

761 **Figure 4**

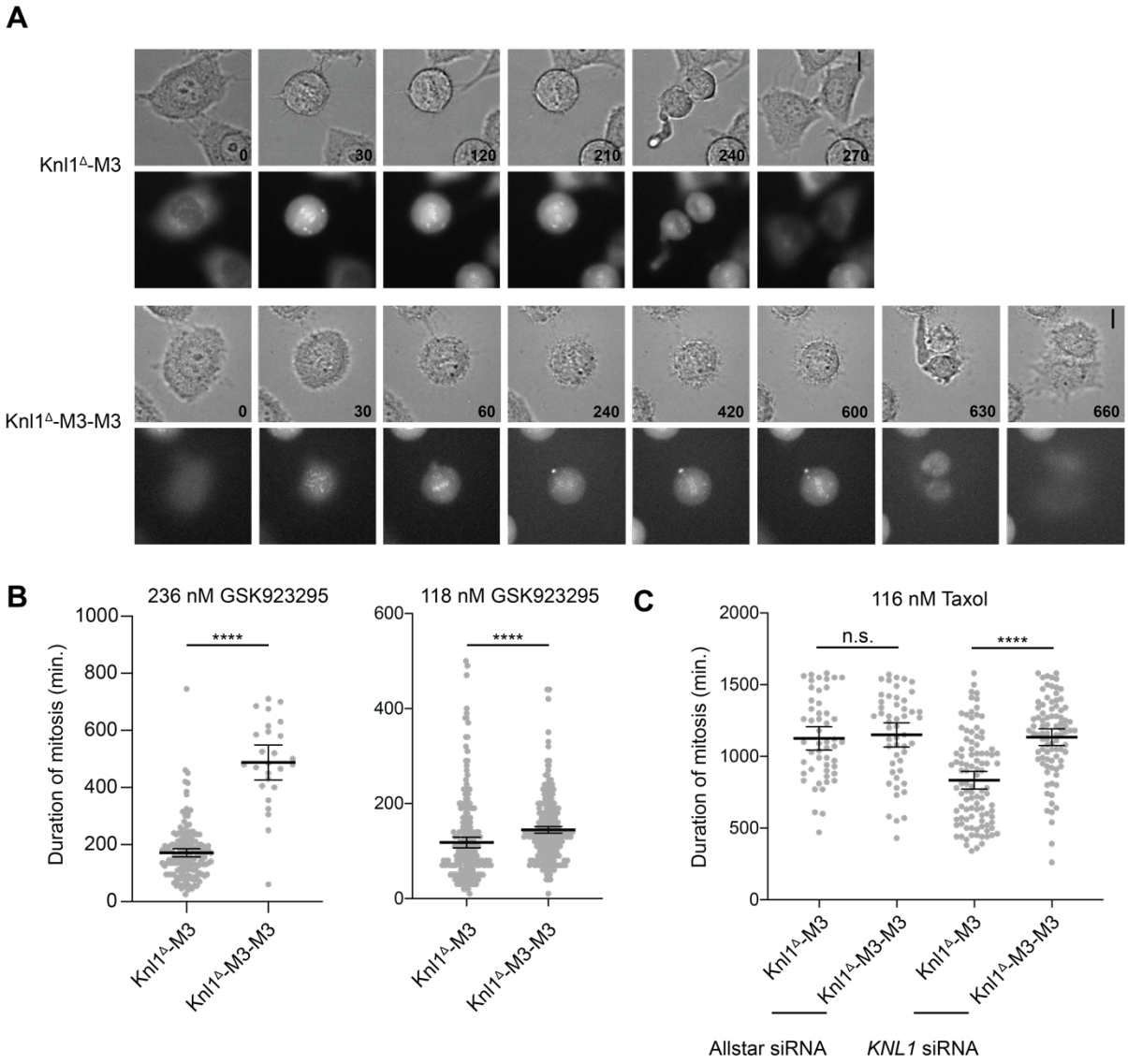

762

763 **Figure 4 – The duration of SAC-induced mitotic delay depends on the number of MELT**
764 **motifs in Knl1.**

765 **(A)** Representative micrographs show mitotic progression of cells with either Knl1$^{\Delta}$-M3 (top) or
766 Knl1$^{\Delta}$-M3-M3 (bottom, scale bar: 10 μm). Time stamps are in minutes.

767 **(B-C)** Duration of mitosis for cells treated with the indicated concentration of GSK923295 and
768 Taxol (left: n = 162 and 26 for Knl1$^{\Delta}$-M3 and Knl1$^{\Delta}$-M3-M3 respectively from two technical repeats;
769 right: n = 235 and 339 for Knl1$^{\Delta}$-M3 and Knl1$^{\Delta}$-M3-M3 respectively, n = 51 and 52 for Allstar siRNA
770 + taxol treatment and n = 102 and 88 for KNL1 siRNA + taxol treatment for Knl1$^{\Delta}$-M3 and Knl1$^{\Delta}$-
771 M3-M3 respectively). Welch's t-test was used to compare the sample means ($p < 0.0001$).

Figure 5

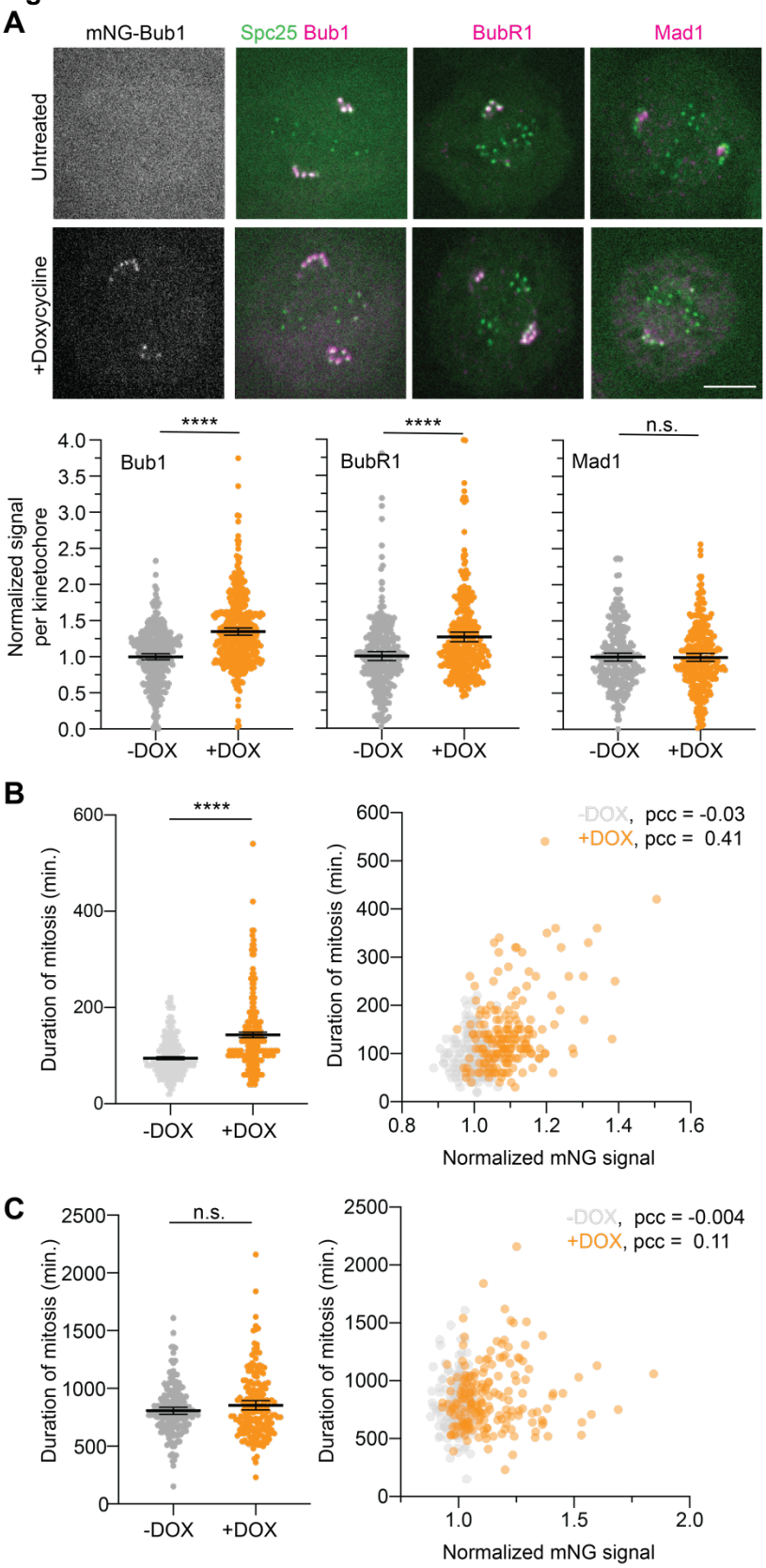
A
mNG-Bub1
Spc25 Bub1
BubR1
Mad1
Untreated
+Doxycycline
Normalized signal per kinetochore
Bub1
BubR1
Mad1
****
****
n.s.
-DOX
+DOX
B
Duration of mitosis (min.)
****
-DOX, pcc = -0.03
+DOX, pcc = 0.41
Normalized mNG signal
C
n.s.
-DOX, pcc = -0.004
+DOX, pcc = 0.11

774 **Figure 5 Bub1 over-expression results in higher recruitment of SAC proteins the**
775 **kinetochore and lengthens the duration of SAC-induced mitotic delay.**

776 **(A)** Top panel: representative fluorescence micrographs of control (top) cells and cells treated
777 with doxycycline to exogenously express mNG-Bub1. Scale bar ~ 4.92 μm. Bottom panel:
778 quantification of immunofluorescence signal per kinetochore for the indicated proteins in
779 control cells and cells treated with doxycycline to induce exogenous mNG-Bub1 expression.
780 Signal values were normalized with the average signal for the respective protein in
781 doxycycline-treated cells. (n = 344 and 390 for Bub1, 346 and 387 for BubR1, and 234 and
782 275 for Mad1 in untreated and doxycycline-treated cells respectively, observations pooled
783 from 3 technical repeats). Welch's t-test used to compare sample means (p-value < 0.0001).
784 **(B)** Left: Quantification of the duration of mitosis in control and doxycycline-treated cells in media
785 containing 25-37 nM GSK923295 (n= 195 and 187 for untreated and doxycycline-treated
786 cells respectively, from 2 technical repeats, Pearson's correlation coefficient (pcc) for each
787 data set noted in the figure). Horizontal lines represent mean ± 95% confidence intervals on
788 the mean. Right: Correlation between the duration of mitosis and the average cellular level
789 of the exogenously expressed mNG-Bub1. mNG-Bub1 signal per cell was normalized with
790 the average signal measured in control cells.
791 **(C)** Left: Quantification of the duration of mitosis in control and doxycycline-treated cells in media
792 containing 330 nM nocodazole (n= 189 and 185 for untreated and doxycycline-treated cells
793 respectively, from 2 technical repeats, Pearson's correlation coefficient (pcc) for each data
794 set noted in the figure). Horizontal lines represent mean ± 95% confidence intervals on the
795 mean. Right: Correlation between the duration of mitosis and the average cellular level of the
796 exogenously expressed mNG-Bub1. mNG-Bub1 signal per cell was normalized with the
797 average signal measured in control cells.

798

799

800 **Figure 6**

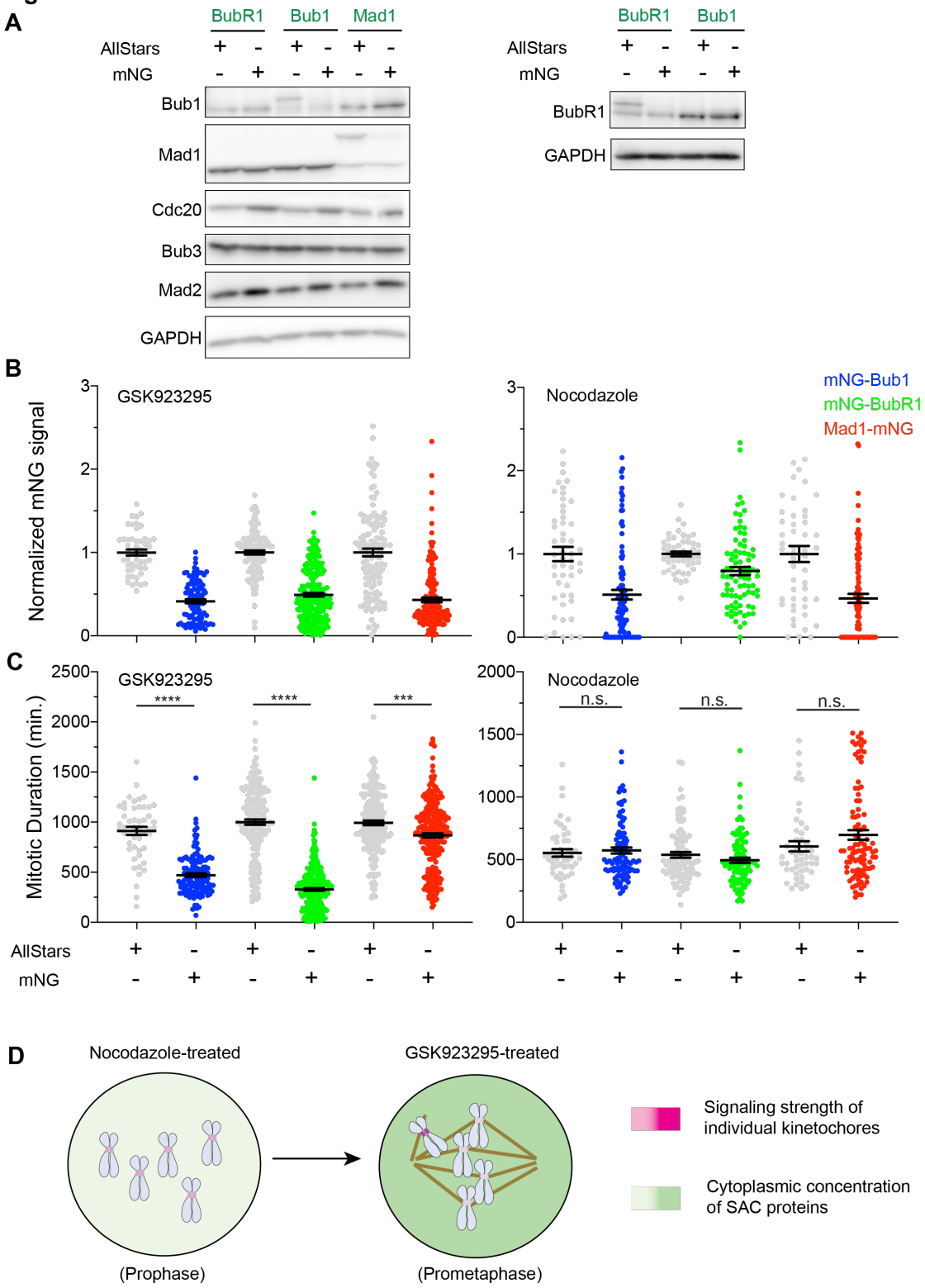

801

802 **Figure 6 The length of SAC-induced anaphase delays is sensitive to partial depletion of**

803 **Bub1 and BubR1, but not Mad1.**

804 **(A)** Western blot analysis of total cell lysates showing that the mNG-tagged SAC protein can be
805 specifically targeted for RNAi using siRNA targeted against mNG.
806 **(B)** Quantification of the mNG-signal per cell under the indicated conditions (For the experiment
807 involving GSK923295 treatment, n = 50, 126, 130 for mNG-Bub1, mNG-BubR1, and Mad1-
808 mNG cells respectively treated with Allstar siRNA and 100, 219, and 177 for mNG-Bub1,
809 mNG-BubR1, and Mad1-mNG cells respectively treated with mNG siRNA; data collected in
810 two technical repeats). For the experiment involving nocodazole treatment, n = 50, 50, and 50
811 for mNG-Bub1, mNG-BubR1, and Mad1-mNG cells respectively treated with Allstar siRNA; n
812 = 100, 85, and 100 for mNG-Bub1, mNG-BubR1, and Mad1-mNG cells respectively treated
813 with mNG siRNA; data collected from 2 technical repeats).
814 **(C)** Quantification of the duration of mitosis for same cells as in B in media containing GSK923295
815 and nocodazole (for GSK923295-treated cells: $p \leq 0.0001$ based on Ordinary one-way
816 ANOVA; for nocodazole-treated cells, $p > 0.253$ based on ordinary one-way ANOVA).
817 **(D)** Model depicts the combined effect of the number of signaling kinetochores per cell and the
818 availability of free, cytoplasmic SAC proteins on the signaling strength of individual
819 kinetochores.

820

821

822 **Figure S1**

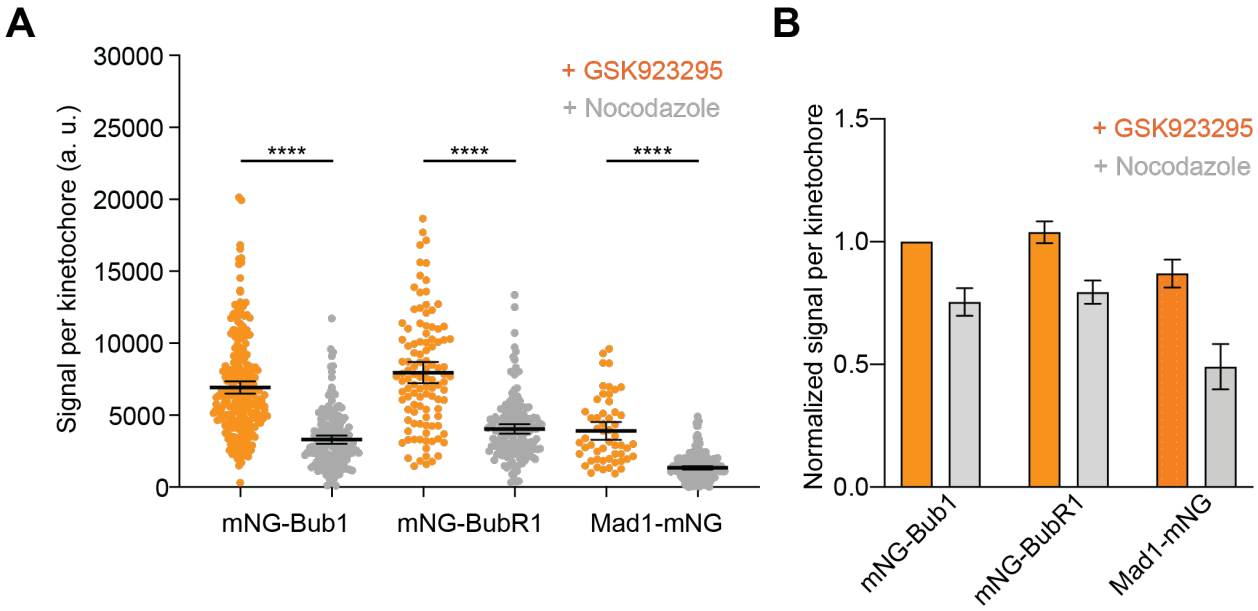

823

824 **Supplementary Figure S1 Effect of ZW10 RNAi on SAC protein recruitment to kinetochores**

825 **(A)** Left: Quantification of the fluorescence signal per signaling kinetochore in cells treated with
826 siRNA against *ZW10* (n = 108, 242, 54 in GSK923295-treated cells and 166, 178, 219 in
827 nocodazole-treated cells for Bub1, BubR1, and Mad1 respectively, pooled from 2 technical
828 repeats).

829 **(B)** Average signals normalized using the mNG-Bub1 signal per kinetochore Horizontal lines
830 display the standard error on the mean ratio.

831

832

833 **Figure S2**

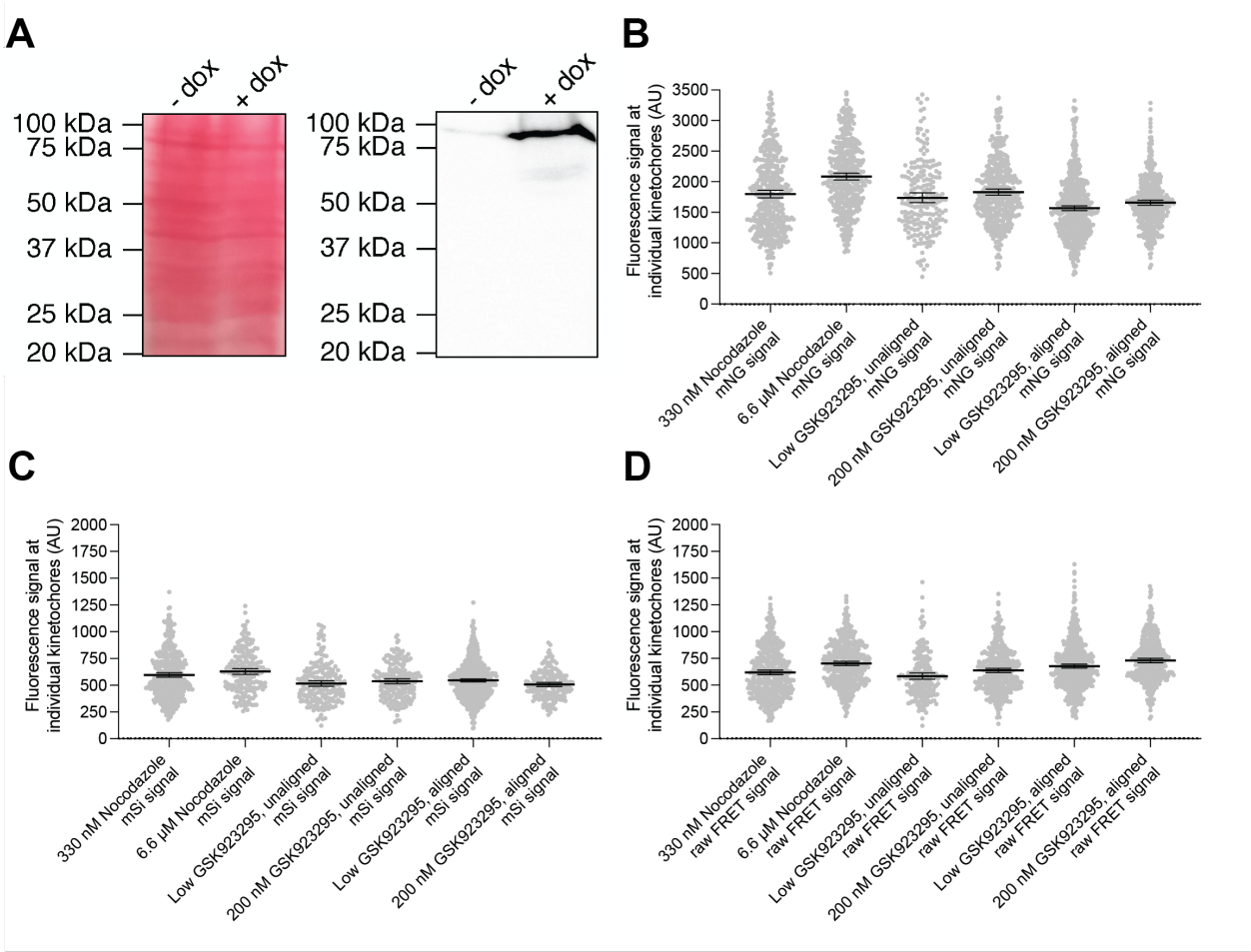

834

835 **Supplementary Figure S2 Characterization of the MPS1sen-KT.**

836 **(A)** Using an antibody against DsRed2 (which detects mScarlet-I), we confirmed that MPS1sen-
837 KT (with a theoretical molecular weight of 97.2 kDa) is expressed as a full-length protein with
838 negligible partial degradation in HeLa A12 treated with doxycycline. A Ponceau S staining of the
839 same blot before membrane blocking (left panel) serves as the loading control.

840 **(B-D)** Raw fluorescence quantification at signaling kinetochores under various drug treatments in
841 the green (B), red (C), and FRET(D) channels. Each gray dot represents a single kinetochore
842 measurement. "Low GSK923295" represents a GSK923295 concentration of 45 nM - 90 nM. Data
843 were compiled from at least two independent experiments (more than 40 cells in total for each
844 group). Mean values ± 95% confidence intervals are overlaid. The variation across different
845 groups may be attributed to not only various FRET efficiencies (which we intend to quantify) but
846 also day-to-day variations of experimental conditions (e.g., the doxycycline-induced expression

847 of MPS1sen-KT). To cancel the effect of these variations, a normalized metric of the FRET
848 efficiency (mNG/FRET; see Methods) was used in this study.

849

850

851 **Figure S3**

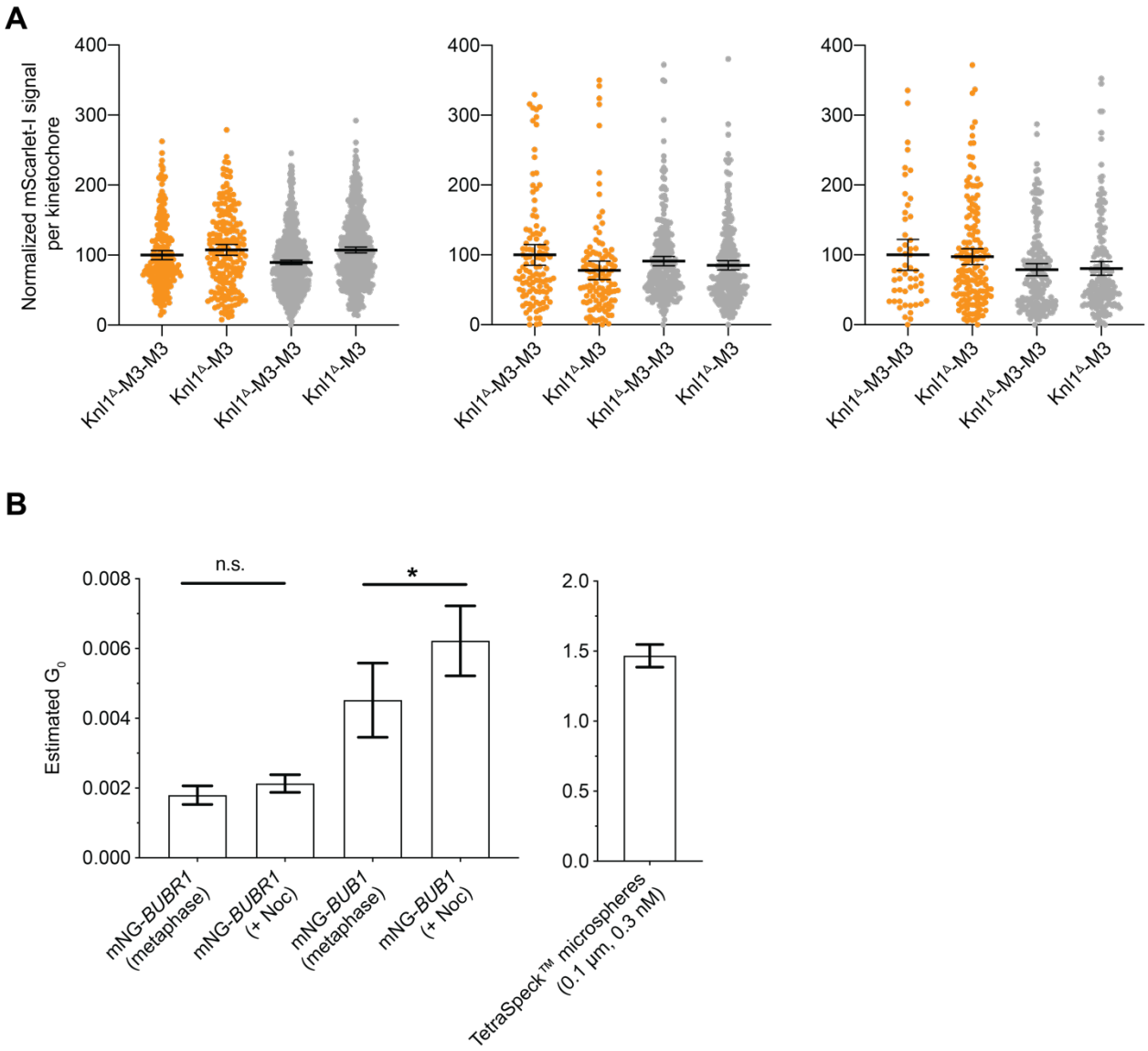

852

853 **Supplementary Figure S3**

854 **A** mScarlet-I fluorescence signal per kinetochore indicating the amount of recombinant Knl1
855 versions (noted by the X-axis labels). Minor differences in the incorporation of the recombinant
856 Knl1 cannot explain the observed differences in SAC protein recruitment in each case. Note that
857 the average value for the mScarlet-I-Knl1$^{\Delta}$-M3-M3 signal was used to normalize the data in each
858 graph.

859 **B** Cytoplasmic abundance of mNG-BubR1 and mNG-Bub1 in metaphase-arrested (MG-132-
860 treated) and nocodazole-treated cells as measured by Fluorescence Correlation Spectroscopy
861 (FCS).

862 **Supplementary Videos**

863 **Video S1 –** Time-lapse imaging of HeLa cells treated with 25 nM GSK923295. Time - hr:min.

864 **Video S2 -** Time-lapse imaging of HeLa cells treated with 25 nM GSK923295 and 1 µg/ml of
865 Doxycycline to exogenously over-express mNG-Bub1. Time - hr:min.

866 **Video S3** - Time-lapse imaging of HeLa cells treated with 330 nM GSK923295. Time - hr:min.

867 **Video S4 -** Time-lapse imaging of HeLa cells treated with 25 nM GSK923295 and 1 µg/ml of
868 Doxycycline to exogenously over-express mNG-Bub1. Time - hr:min.

869 **Video S5 –** Time-lapse imaging of genome-edited HeLa cells heterozygous for mNG-Bub1 and
870 exogenously expressing H2B-mCherry. Cells were released from a G1/S block into media
871 containing 236 nM GSK923295. Time - hr:min.

872 **Video S6 –** Time-lapse imaging of genome-edited HeLa cells heterozygous for mNG-Bub1 and
873 exogenously expressing H2B-mCherry. Cells were treated with siRNA targeting mNG to partially
874 deplete BubR1 and released from a G1/S block into media containing 236 nM GSK923295. Time
875 - hr:min.